Dynamic and structural signatures of lamellar actomyosin force generation

Yvonne Aratyn-Schaus[a], Patrick W. Oakes[a,b], and Margaret L. Gardel[a,b]
[a]Institute for Biophysical Dynamics and [b]James Franck Institute and Department of Physics, University of Chicago, Chicago, IL 60637

ABSTRACT **The regulation of cellular traction forces on the extracellular matrix is critical to cell adhesion, migration, proliferation, and differentiation. Diverse lamellar actin organizations ranging from contractile lamellar networks to stress fibers are observed in adherent cells. Although lamellar organization is thought to reflect the extent of cellular force generation, understanding of the physical behaviors of the lamellar actin cytoskeleton is lacking. To elucidate these properties, we visualized the actomyosin dynamics and organization in U2OS cells over a broad range of forces. At low forces, contractile lamellar networks predominate and force generation is strongly correlated to actomyosin retrograde flow dynamics with nominal change in organization. Lamellar networks build ~60% of cellular tension over rapid time scales. At high forces, reorganization of the lamellar network into stress fibers results in moderate changes in cellular tension over slower time scales. As stress fibers build and tension increases, myosin band spacing decreases and α-actinin bands form. On soft matrices, force generation by lamellar networks is unaffected, whereas tension-dependent stress fiber assembly is abrogated. These data elucidate the dynamic and structural signatures of the actomyosin cytoskeleton at different levels of tension and set a foundation for quantitative models of cell and tissue mechanics.**

Monitoring Editor
Alexander Mogilner
University of California, Davis

Received: Nov 10, 2010
Revised: Jan 18, 2011
Accepted: Jan 31, 2011

INTRODUCTION

In adherent cells, forces generated within the actin cytoskeleton are transmitted at focal adhesions and result in traction forces on the extracellular matrix (ECM) (Burridge and Chrzanowska-Wodnicka, 1996; Parsons *et al.*, 2010). The regulation of cellular traction force is fundamental to cell adhesion, motility, and extracellular matrix remodeling (Bershadsky *et al.*, 2003; Discher *et al.*, 2005; Geiger *et al.*, 2009; Gardel *et al.*, 2010). Near the cell periphery within the lamellipodium, polymerization of densely branched F-actin networks drives F-actin retrograde flow that coincides with focal adhesion assembly (Alexandrova *et al.*, 2008; Choi *et al.*, 2008; Gardel *et al.*, 2008). The traction stresses transmitted at these nascent, myosin-independent lamellipodial adhesions are small (Gardel *et al.*, 2008; Aratyn-Schaus and Gardel, 2010; Fournier *et al.*, 2010). Proximal to the lamellipodium, myosin II motors generate contractile forces on F-actin which both modulate F-actin dynamics and organize the lamellar actin cytoskeleton into networks and bundles that generate large traction stresses on the ECM (Gardel *et al.*, 2010). There is a qualitative understanding of the interplay among myosin II activity, lamellar actin organization, and traction force generation. When myosin activity is inhibited, the actin cytoskeleton is organized into a lamellar network that generates low force, while high myosin activity results in stress fibers that generate high tension (Chrzanowska-Wodnicka and Burridge, 1996; Balaban *et al.*, 2001; Beningo *et al.*, 2006). However, a quantitative biophysical understanding of how lamellar F-actin dynamics and organization regulate the extent of cellular force generation is largely unknown. This knowledge is sorely needed to elucidate the physical mechanisms of cellular force generation and to build predictive physical models of cells and tissues.

Contractile lamellar networks, or "contractile-network arrays," are composed of randomly polarized actin filaments interspersed with submicrometer puncta of myosin II motors (Verkhovsky *et al.*, 1995, 1997; Svitkina *et al.*, 1997). The spatial coordination of F-actin

This article was published online ahead of print in MBoC in Press (http://www.molbiolcell.org/cgi/doi/10.1091/mbc.E10-11-0891) on February 9, 2011.

Address correspondence to: Margaret L. Gardel (gardel@uchicago.edu).

Abbreviations used: ECM, extracellular matrix; FFT, fast Fourier transform; GFP, green fluorescent protein; MLC, myosin light chain; PAA, polyacrylamide.

© 2011 Aratyn-Schaus *et al.* This article is distributed by The American Society for Cell Biology under license from the author(s). Two months after publication it is available to the public under an Attribution–Noncommercial–Share Alike 3.0 Unported Creative Commons License (http://creativecommons.org/licenses/by-nc-sa/3.0).

"ASCB®," "The American Society for Cell Biology®," and "Molecular Biology of the Cell®" are registered trademarks of The American Society of Cell Biology.

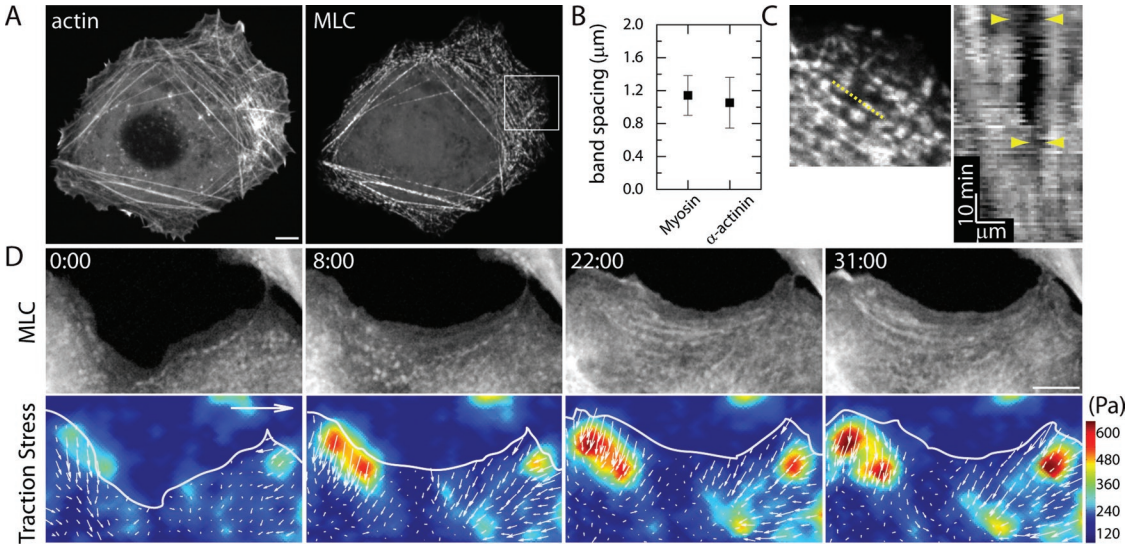

FIGURE 1: Transitions between lamellar networks and stress fibers occurs near the periphery of spread cells. (A) Images of mApple-actin and GFP-MLC (myosin light chain), used to visualize myosin II, in a U2OS cell. Scale bar, 5 μm. (B) Average center-to-center band spacing for myosin (n = 24 band pairs within three cells) and α-actinin (n = 16 band pairs within two cells) along actin bundles. Error bars indicate SE. (C) Left, image is the region of interest indicated by box in (A), with a dashed yellow line indicating bundle used to generate kymograph. Right, a kymograph generated from images along the line scan in the image on the left and stacked over time. The yellow arrows indicate locations of two neighboring myosin bands during stress fiber formation. (D) Top, time-lapse images of GFP-MLC; bottom, underlying traction stress during cell protrusion. Traction stress vectors are overlaid as white arrows on top of heat scale images, which indicate the stress magnitudes. Vector scale bar, 400 Pa; distance scale bar, 5 μm. Time indicated in min:s.

assembly dynamics and myosin II activity within lamellar networks results in coherent, continuous flow of F-actin away from the cell periphery (Vallotton *et al.*, 2004; Schaub *et al.*, 2007). In the absence of focal adhesions, the rate of retrograde flow is 100 nm/s (Alexandrova *et al.*, 2008; Zhang *et al.*, 2008), similar to the unloaded velocity of myosin IIA (Cuda *et al.*, 1997). In the presence of focal adhesions, this retrograde flow is markedly reduced to ~10–20 nm/s (Giannone *et al.*, 2004; Hu *et al.*, 2007; Alexandrova *et al.*, 2008) and it is thought that tension sustained at adhesions assists in remodeling lamellar networks into bundles (Verkhovsky and Borisy, 1993). However, direct measurements of forces involved during lamellar remodeling into stress fibers are lacking.

F-actin cross-linking by myosin IIA and α-actinin assist in the formation of a variety of contractile F-actin bundles (Cramer, 1999; Hotulainen and Lappalainen, 2006; Gardel *et al.*, 2010). Stress fibers, reminiscent of sarcomeric structures in striated muscle, are characterized by short actin filaments of alternating polarity decorated with periodic bands of myosin and α-actinin (Peterson *et al.*, 2004; Naumanen *et al.*, 2008). It was proposed that α-actinin–mediated bundling of F-actin occurs as the first step of stress fiber formation, creating an F-actin architecture against which myosin can efficiently generate force (Hotulainen and Lappalainen, 2006; Naumanen *et al.*, 2008). However, because stress fiber assembly in spread cells occurs predominately in a small region near the cell periphery, our understanding of the sequential steps of force-dependent stress fiber assembly is incomplete.

Here we quantified the lamellar F-actin organization and dynamics at different levels of cellular force generation. By dynamically modulating myosin activity, we observed the transition from contractile lamellar networks to stress fibers occurring across the entire lamella of individual cells within a single experiment. By combining high-resolution quantitative imaging of the lamellar cytoskeleton with traction force microscopy, we were able to correlate lamellar F-actin dynamics and organization to the total cellular force generated. Quite surprisingly, we found that lamellar networks generated up to 60% of the maximum forces generated. In lamellar networks, changes in force output were dominated by changes in lamellar retrograde flow dynamics with very little change in lamellar organization. The remainder of the cellular force (~40%) was generated as lamellar networks remodeled into stress fibers over significantly longer time scales. During myosin-mediated remodeling of F-actin into bundles, α-actinin accumulated onto bundles in a banded pattern. The spacing of myosin and α-actinin bands decreased as force was built. On soft matrices, which inhibit stress fiber formation, lamellar network force generation was unaffected. Altogether, our data suggest that a contractile lamellar actin network can act as a prominent force generator, allowing for the rapid growth of cellular tension in the absence of stress fibers. At higher force levels, stress fiber formation is correlated with further increases in force over much longer time scales. These results identify the dynamic and structural signatures of force generation by the actomyosin cytoskeleton and provide the foundation for biophysical models of cellular contractility.

RESULTS

Formation and remodeling of stress fibers in U2OS osteosarcoma cells

To visualize the dynamics of the lamellar cytoskeleton, we coexpressed mApple-actin and green fluorescent protein–myosin light chain (GFP-MLC) (Figure 1A) in U2OS osteosarcoma cells plated on fibronectin-coated glass coverslips and acquired time-lapse fluorescence images using a spinning-disk confocal microscope. As previously observed, U2OS cells prominently display stress fibers, identified by actin bundles with periodic bands of myosin (Figure 1A). In portions of stress fibers devoid of myosin, α-actinin is localized (Supplemental Figure 1). Thus stress fibers are characterized by alternating bands of α-actinin and myosin occurring at intervals of 1.1 ± 0.2 μm and 1.0 ± 0.3 μm, respectively (Figure 1B) (Peterson *et al.*, 2004; Hotulainen and Lappalainen, 2006). Although stress fibers can

be further classified by their orientation with respect to the cell edge and F-actin assembly mechanisms (Hotulainen and Lappalainen, 2006), we identify stress fibers by using this characteristic spacing of myosin and α-actinin bands.

In spread cells, stress fiber assembly occurs near the lamellipodium–lamella interface (Hotulainen and Lappalainen, 2006). As previously described, myosin puncta appear near the lamellipodial base, undergo retrograde motion, and coalesce into bands along an actin bundle (Supplemental Movie 1). During assembly and retrograde motion of stress fibers, the spacing between myosin bands decreases from 2 to 1 μm (Supplemental Movie 1, Figure 1C).

To directly correlate stress fiber assembly with changes in cellular traction force, we imaged cells expressing GFP-MLC spread on fibronectin-coated polyacrylamide gels for the application of traction force microscopy (Sabass *et al.*, 2008). Over similar time scales of stress fiber assembly, traction stresses in two discrete foci, presumed to underlie focal adhesions, were observed to increase nearly twofold (Figure 1D). Because a component of the traction stress vectors pointed in the direction of newly formed stress fibers, it is likely that this change in stress could be attributed to stress fiber formation. However, because numerous modes of cytoskeletal organization and dynamics occurred within nearby regions simultaneously, local correlations between changes in traction stress and stress fiber assembly were limited.

Substantial traction is exerted prior to F-actin bundle formation

To facilitate measurements of F-actin cytoskeletal organization at different levels of cellular tension, cellular contractility was dynamically perturbed by incubation of cells with blebbistatin, a pharmacological inhibitor of myosin II ATPase activity (Straight *et al.*, 2003). It is well established that myosin inhibition abolishes actin bundles, decreases focal adhesion size, and reduces traction stress (Balaban *et al.*, 2001; Beningo *et al.*, 2006; Gardel *et al.*, 2008). Moreover, it is known that removal of this inhibition induces stress fiber assembly, focal adhesion elongation, and increased traction stress (Chrzanowska-Wodnicka and Burridge, 1996; Katoh *et al.*, 2007). However, quantitative measurements to assess the changes in actin organization and dynamics while measuring cellular traction force have been lacking.

A 30-min incubation of U2OS cells in media containing 50 μM blebbistatin eliminated actin bundles, decreased focal adhesion size, and reduced traction stress (Figure 2A, Supplemental Figure 1B, Supplemental Movie 2). Myosin II activity was restored uniformly across the cell by washing out blebbistatin-containing media and rapidly inactivating any residual drug by blue light imaging (Sakamoto *et al.*, 2005). Within 3 min of blebbistatin removal, dim F-actin bundles appeared throughout the cell and were identified by linear structures with an enhanced intensity relative to the surrounding cytoplasm. During this time, the formation of peripheral F-actin bundles coincided with the elongation of focal adhesions at which bundles terminated (Supplemental Figure 1B) (Hotulainen and Lappalainen, 2006; Choi *et al.*, 2008; Aratyn-Schaus and Gardel, 2010). Central bundles were often interconnected into the surrounding cytoskeleton rather than directly anchored to focal adhesions localized to the cell periphery (Hotulainen and Lappalainen, 2006). Several minutes after stimulation of myosin ATPase activity, focal adhesions reached a constant length while F-actin bundles continued to increase in number. Within 15–20 min, a bundled F-actin cytoskeleton similar to control cells was restored. To quantify the linear bundle density, we calculated the number of bundles per μm and found that the density of bundles increased from zero immediately after blebbistatin removal to ~0.6 bundles per μm within 20 min (Figure 2B). These data could be well fit to a single exponential with a half-time of 8 min, reflecting a time scale of myosin-dependent actin bundle formation in U2OS cells.

As new bundles formed, the GFP-actin intensity of individual bundles also increased. Transverse line scans across bundles in GFP-actin images showed clear peaks of actin intensity within the bundle, I_b, compared with that of the surrounding cytoplasm, I_c. After correction for photobleaching, the intensity of the cytoplasmic pool did not change over time (unpublished data). By contrast, the ratio of bundle intensity to the surrounding cytoplasm intensity, I_b/I_c, did change, increasing from a ratio of 1 at time zero, indicating that no bundles were detected, to a ratio of 1.5 ~15 min after myosin reactivation (Figure 2C). Thus stimulation of contractility induced thickening of individual bundles such that the amount of F-actin contained within individual bundles increased.

As an independent quantitative measure of the formation of strongly aligned F-actin structures in the cell, we developed an algorithm to measure the local order parameter in small (~6 μm^2) regions of GFP-actin images. This order parameter utilizes information from the image Fourier transform to assess the existence and extent of linear alignment in the image region, with a value of 0 corresponding to a homogeneous region with random alignment and a value of 1 corresponding to a fully parallel arrangement. Indeed regions in the GFP-actin images with actin bundles had an order parameter larger than 0.8, whereas regions with fewer bundles had an order parameter less than 0.5 (Figure 2A, Supplemental Movie 2). We then calculated the average order parameter in the cell as a function of time after blebbistatin removal (Figure 2D). The average order parameter was markedly decreased for blebbistatin-treated cells compared with control cells. On removal of blebbistatin, the average order parameter increased from ~0.45 to 0.65 over a period of 20 min. These data could be well fit to a single exponential with a half time of 10 min. Thus all three quantitative metrics of F-actin organization indicate that myosin-dependent remodeling of the lamellar network into stress fibers occurred over a 15–20 min time scale. This remodeling consisted of both the de novo formation of actin bundles and the increased intensity of existing bundles.

To simultaneously quantify cellular tension, the total cellular traction force exerted by the cell was measured during myosin-dependent remodeling. Within 3 min of blebbistatin removal, significant peripheral traction stresses were observed (Figure 2A) and the total cellular traction force increased from 120 to 240 nN (Figure 2E). Thereafter, in ~60% of cells observed, the cellular traction force continued to slowly increase. In the remaining cases, traction forces reached a steady state within 3 min of drug removal (unpublished data). The increase of the traction force after removal of blebbistatin could be well fit to a double exponential, composed of a "rapid" growth phase with a half time of ~30 s and a "slow" growth phase with a half time of 10 min. During the rapid phase, ~60–70% of traction recovered while the slow phase coincided with an additional 30–40% increase of cellular traction force (Figure 2E). Strikingly, the rapid recovery of cellular traction forces preceded the formation of bundled F-actin. The time scales of actin bundle formation and the slow phase of traction recovery were similar.

Rapid increase in tension occurs with diminished rates of myosin motion

Since significant traction force was generated with little change in lamellar actin organization, we speculated that myosin-driven actin dynamics may play an important role. After treatment with 50 μM blebbistatin, myosin puncta were intact and distributed throughout

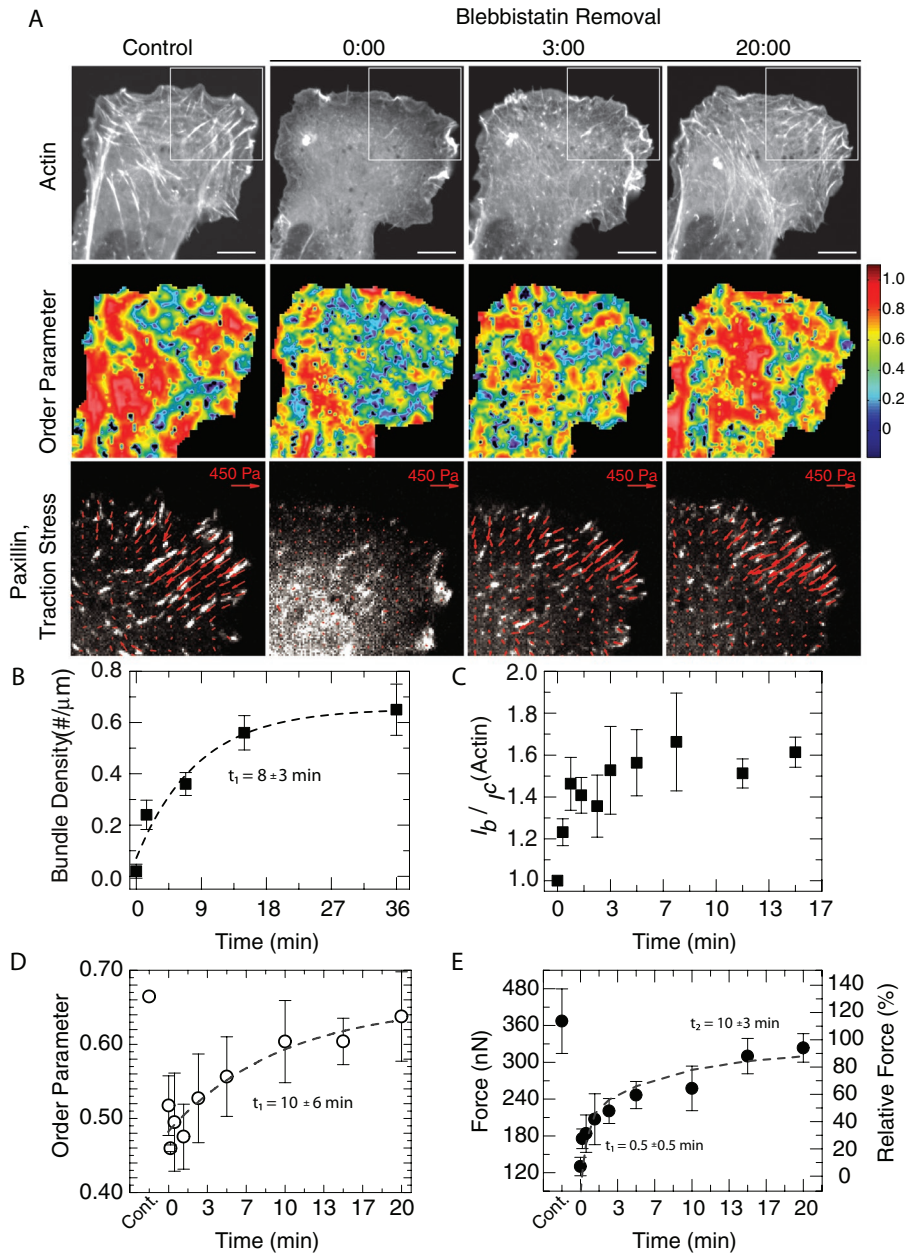

FIGURE 2: Dynamic coordination of F-actin remodeling with changes in traction force. (A) Top, GFP-actin images before (control) and after treatment and removal of blebbistatin. Scale bar, 10 μm. Middle, pseudocolor images of the order parameter calculated from GFP-actin images shown above, with red representing the highest order and blue representing the lowest order. Bottom, images of mApple-paxillin for the region of interest indicated by white box in GFP-actin images with traction stress vectors (red arrows) overlaid. Vector scale bar, 150 Pa. Time indicated in min:s. (B) The mean linear density of actin bundles vs. time after blebbistatin removal. Dashed line indicates a fit of the data with a single exponential, with a time scale, t_1, of 8 ± 3 min. Error bars indicate SE, with a sample size of 31 bundles within three cells. (C) The ratio of the peak GFP-actin intensity within bundles, I_b, to the GFP-actin intensity of the surrounding cytoplasm, I_c, as a function of time after blebbistatin removal, with each data point representing 9–12 bundles within three cells. (D) Order parameter as a function of time prior to and after blebbistatin removal. Dashed line indicates fit of data to a single exponential with a time scale of 10 ± 6 min. Data reflect mean and SE from n = 4 cells. (E) Total cellular traction force prior to and after blebbistatin removal. The relative force, calculated as a percentage, that is used in subsequent figures is shown on the right-hand axis. Dashed line indicates a fit to a double exponential with a fast time scale of t_1 = 0.5 ± 0.5 min and a slower time of t_2 = 10 ± 3 min. Data reflect mean and SE from n = 10 cells.

the lamella and cell body (Figure 3A, Supplemental Movie 3). Three minutes after blebbistatin removal, myosin puncta became associated with dim actin bundles. By 20 min, linear bands of myosin colocalized with bright actin bundles. Thus rearrangement of myosin coincided with the formation of actin bundles.

To quantify myosin dynamics during blebbistatin removal, we used customized image processing algorithms to identify the centroid and movement of myosin puncta with submicrometer accuracy (Ji and Danuser, 2005). We found that myosin motion corresponded closely to actin motion. In the first 30 s after blebbistatin removal, myosin puncta throughout the cell underwent rapid movement with an average speed of ~20 nm/s and a maximal speed of ~60 nm/s (Figure 3, B and C). Within ~5–10 μm of the cell periphery in the lamella, coherent retrograde motion of myosin was observed (Figure 3B). Closer to the cell center in the cell body, the direction of flow was characterized by locally coherent movement toward foci of contraction (Figure 3B). Within 2 min after blebbistatin removal, the average myosin speed decreased to ~5 nm/s, the typical F-actin speed observed in stress fibers of U2OS cells in control conditions (Hotulainen and Lappalainen, 2006). Similar to flow patterns observed at early times, coherent retrograde flow was observed in the lamella but the direction of flow varied widely in the cell body.

Strikingly, the decrease in average myosin speed occurred over a similar time scale as the rapid phase of traction force recovery observed in Figure 2E. Indeed a strong inverse correlation between traction force and myosin speed was observed for the initial fast phase of tension buildup (Figure 3D). This correlation diminished at longer times as the traction forces continued to increase while the myosin speed remained constant. Thus the initial stages of force buildup coincided with diminished rates of movement. These changes in actomyosin retrograde flow dynamics coincided with the recovery of ~60% of the total cellular traction force and preceded the formation of actin bundles.

Myosin II drives local remodeling during bundle formation

The formation of stress fibers occurred over a period of 10–20 min after myosin motion reached a steady state (Figure 3C). The steps in stress fiber assembly were qualitatively similar across the cell. During the rapid phase of traction increase after blebbistatin removal, myosin puncta

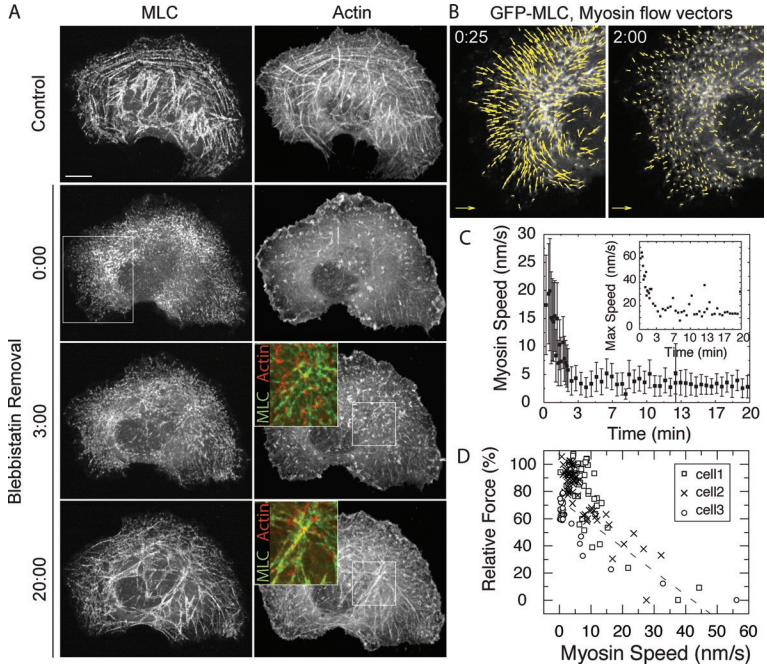

FIGURE 3: Rapid force generation is inversely correlated to lamellar retrograde flow speed. (A) Images of (left) GFP-MLC and (right) mApple-actin before (Control) and after removal of blebbistatin. Insets show color combine images at 3:00 and 20:00, which reveal colocalization of MLC (green) and F-actin (red) for regions outlined by white boxes in the bottom panel. Scale bar, 10 μm. Time indicated in min:s. (B) Images of GFP-MLC from region of interest indicated by white rectangle in the MLC image at 0:00 overlaid with corresponding flow vectors (yellow) obtained at 25 s and 2 min after blebbistatin removal. Vector scale, 30 nm/s. (C) Average myosin flow speed vs. time after blebbistatin removal. Data reflect mean and SE from ~500 flow vectors. Inset, maximum myosin speed over the same times. (D) Relative force vs. average myosin flow speed with different symbols indicating data obtained for three representative cells. Each data point reflects the mean of more than one hundred flow measurements. A strong inverse relationship is observed between 0 and 60% force (Pearson r = −0.79), and the dashed line indicates the best linear fit to these data.

moved into linear arrangements that colocalized with thin actin bundles (Figure 4A). After the formation of linear structures, myosin puncta continued to reorganize, and the degree of coherency of myosin movement in different regions changed over time. Local motions of myosin puncta were influenced by movements in neighboring bundles, appearing to undergo a "tug of war" between different areas of the actomyosin network (Figure 4B, 03:30 and 09:30). Myosin bands along bundles did not always move in the same direction, with antiparallel movement of bands along single bundles resulting in local extensions (Figure 4B, 13:30). At even later times following blebbistatin inactivation, the flow of myosin bands appeared to become coordinated once again (Figure 4B, 14:30).

Although locally both extensile and contractile remodeling occurred, the bundles formed were, overall, contractile, with the length of bundles decreasing at a rate of ~1.6 nm/s (Figure 4A). This contraction coincided with an overall decreased spacing of myosin bands along the bundle, as observed in Figure 4A and in the kymograph in Figure 4C. Interestingly, no significant reduction in myosin band spacing was observed as the total force generated by the cell increased from 0–50%, coinciding with the rapid phase of tension buildup (Figure 4D). By contrast, as the traction force generated increased from 50–100%, the spacing of myosin bands decreased from ~1.8 to 1.2 μm, the value observed in control conditions (Figure 1D). Thus a nearly twofold reduction in myosin band spacing correlated with the slow phase of traction buildup, which occurred at the highest levels of tension.

Recruitment of α-actinin to actomyosin bundles occurs at high tension

In contrast to myosin, no prominent α-actinin bands remained after blebbistatin treatment (Figure 5A, Supplemental Movie 4), consistent with previous observations (Katoh *et al.*, 2007). In the rapid phase of traction recovery, which occurred in the first minutes after blebbistatin removal, there was very little change in α-actinin localization. As faint actin bundles formed, α-actinin accumulated onto bundles in sparse and faint bands (Figure 5A, 02:00). As the actin intensity within bundles increased over time, prominent α-actinin bands became apparent (Figure 5A, 07:00–35:00). A kymograph of α-actinin intensity along a bundle during tension buildup shows the initial appearance and subsequent increased intensity and density of α-actinin bands around 7 min (arrows, Figure 5B).

The number of α-actinin bands observed per unit length of actin bundle remained close to zero when the extent of traction force generation was less than 50% and started to increase at higher force levels (Figure 5C). At these higher values of cellular tension, the average spacing of α-actinin bands was similar to those observed for the myosin bands at similar tension, decreasing from 1.4 to 1.1 μm as the force generated increased from 70–100% (Figure 5D). These results are consistent with the decreased α-actinin band spacing observed after enhanced myosin activity (Peterson *et al.*, 2004). In contrast to myosin, this reduced spacing occurred through the de novo assembly of new α-actinin bands rather than local remodeling events.

In addition to the formation of new α-actinin bands, the intensity of individual α-actinin bands also increased. The relative intensity of α-actinin band intensity compared with the surrounding cytoplasm increased from 1.0 at low force levels to 1.6 at high force levels (Figure 5E). This finding suggests that α-actinin accumulation into bands during stress fiber assembly is also tension-dependent.

Force generation by contractile lamellar network is unaffected by ECM stiffness

Previous experiments showed that extracellular matrix compliance can have a profound impact on the organization of the actin cytoskeleton such that lamellar networks predominate on soft matrices and stress fibers predominate on sufficiently stiff matrices (Yeung *et al.*, 2005). To explore how modifying extracellular tension affected the dynamics of lamellar actin force generation, we plated cells on fibronectin-coated polyacrylamide gels with a shear elastic modulus of 0.6 kPa. On soft matrices, the extent of bundles within the lamellar actin cytoskeleton was markedly reduced and focal adhesion size was decreased (Figure 6A). The total traction force generated by cells also decreased by ~30% to 240 nN (Figure 6, A and B, "Control").

After blebbistatin treatment, there were no differences between lamellar organization, focal adhesion size, and traction forces for cells plated on the two different gel stiffnesses. On removal of the blebbistatin, traction forces built up rapidly for cells plated on soft substrates within 1 min after drug removal (Figure 6B). Following this rapid force buildup, no significant changes in force generation

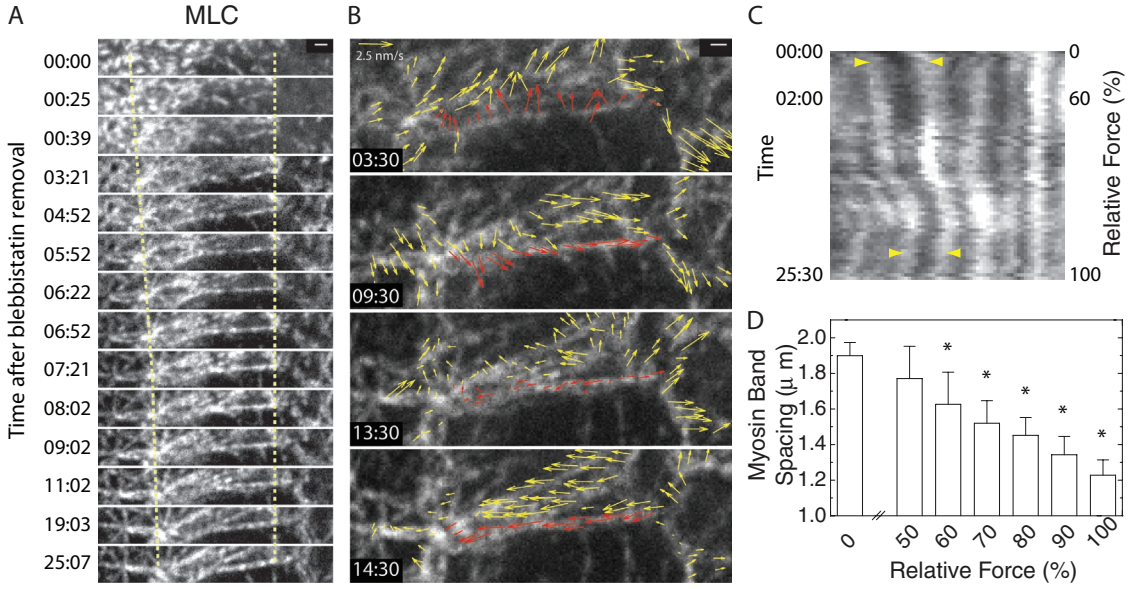

FIGURE 4: Remodeling of myosin bands during bundle formation. (A) Images of GFP-MLC after blebbistatin removal showing typical process of stress fiber formation. Scale bar, 1 μm. Times indicate min:s. Dashed lines indicate locations of terminal ends of the same bundle over time. (B) Images of GFP-MLC with overlaid flow vectors across several time points during stress fiber formation. Red vectors indicate bands within a bundle of interest; yellow vectors indicate bands within surrounding bundles. Scale bar, 1 μm; flow vector scale bar, 2.5 nm/s. Times indicated in min:s. (C) Kymograph of a line scan of GFP-MLC along a bundle as a stress fiber is formed after blebbistatin removal, with high-intensity streaks revealing the location of myosin bands. Relative force indicated on right-hand axis. Yellow arrows indicate locations on neighboring myosin bands at early times (low force) and late times (high force). (D) Average myosin band spacing along bundles vs. relative cellular traction force. Data reflect mean and SD for n = 10–47 pairs of myosin bands within three cells. The * indicates p-values < 0.05 between data and data obtained at 0%, as calculated by Student's *t* test.

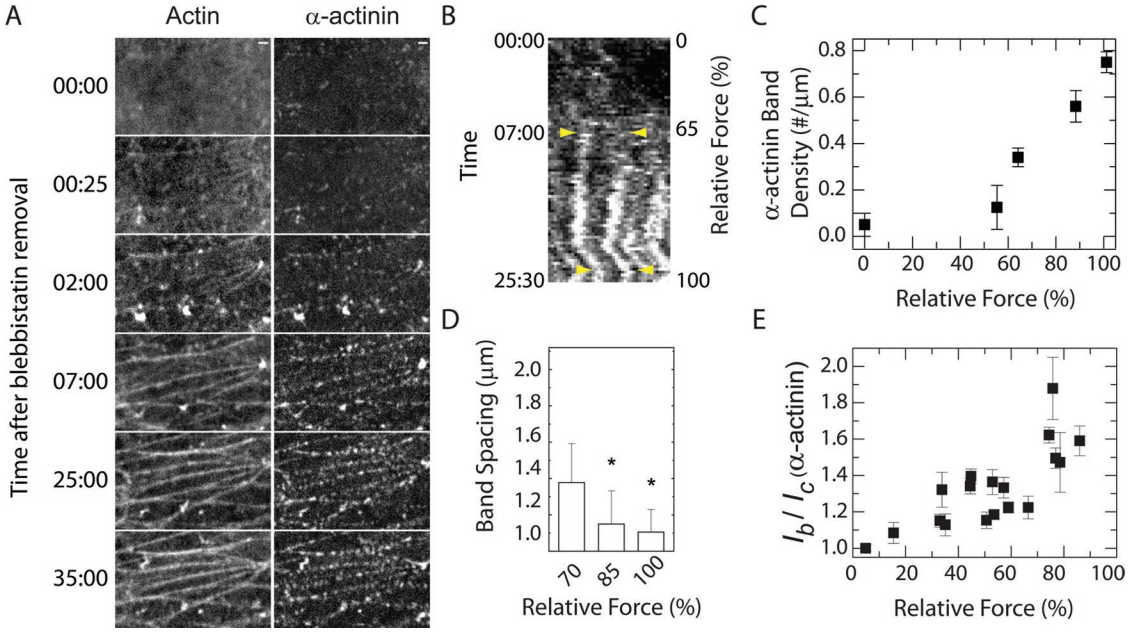

FIGURE 5: α-Actinin bands form and intensify during stress fiber formation. (A) Images of mApple-actin and GFP-α-actinin over time after blebbistatin removal. Time indicated in min:s. Scale bar, 1 μm. (B) Kymograph of a line scan along an actin bundle over time after blebbistatin removal. High-intensity streaks indicate the location of α-actinin bands along the bundle. The yellow arrows indicate the location of two neighboring bands at the average time of appearance along the bundle (7:00) and at later times. Relative force is indicated on the right-hand axis. (C) Average linear density of α-actinin bands in bundles as a function of force. Error bars indicate SE from a sample size of 35 bundles within three cells. (D) Bar chart of α-actinin band spacing as a function of force. The absence of bands precludes measurements at lower forces. Error bars indicated SD about the mean for a sample size, n = 7, 8, and 24 α-actinin band pairs for 70%, 85%, and 100% force recovered, respectively. The * indicates p-values < 0.05 between the data and data obtained at 70% force recovery, as determined by Student's *t* test. (E) Peak intensity of GFP-α-actinin band, I_b, relative to the surrounding cytoplasm, I_c, as a function of relative force. Data reflect mean and SE from 24–60 bands in three cells.

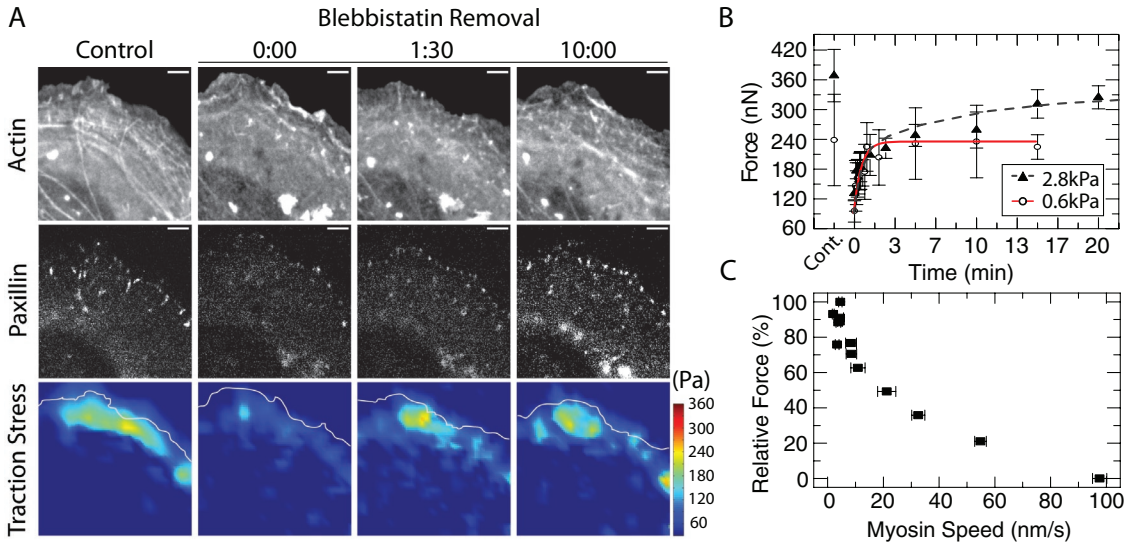

FIGURE 6: Dynamic coordination of F-actin remodeling with changes in traction force on soft matrices. (A) Images of (top) GFP-actin and (middle) mApple-paxillin before (Control) and after treatment and removal of blebbistatin for U2OS cells plated on a PAA gel with stiffness of 0.6 kPa. Heat maps of traction stresses (bottom) underlying focal adhesions, with stress magnitude scale on the right. Time indicated in min:s. Scale bar, 5 μm. (B) Total cellular traction force prior to and after blebbistatin removal for stiff (2.8 kPa) and soft (0.6 kPa) gels. Dashed line indicates a fit to a double exponential for force recovery on stiff gels and red line indicates a fit to a single exponential for force recovery on soft gels, showing nearly identical recovery at fast time scales. Error bars indicate the SE with a sample size of n = 10 cells for 2.8 kPa gel and n = 4 cells for 0.6 kPa gel. (C) Relative force vs. average myosin flow speed on soft (0.6 kPa) gels.

or lamellar actin organization were observed in any of the cells imaged. Quite strikingly, the dynamics of the rapid force buildup was quantitatively similar for the soft and stiff matrices; cells built up the same magnitude of force over similar time scales (Figure 6B).

During the period of rapid traction force buildup, the actin retrograde flow decreased from ~100 to 5 nm/s (Figure 6C). Thus the rapid force generation by lamellar networks was not affected by extracellular matrix mechanics. However, the nominal force buildup associated with lamellar remodeling into stress fibers was absent.

DISCUSSION

In this study, we characterized the dynamics and organization of F-actin, myosin, and α-actinin in the formation of contractile lamellar networks and stress fibers that generate and sustain varying levels of cellular tension. Altogether we describe two distinct phases of tension buildup: the first, at low tension, is governed primarily by changes in lamellar actomyosin dynamics; the second, at higher tension, is governed primarily by the remodeling of lamellar networks into stress fibers.

At the lowest force levels, the lamellar actomyosin network underwent rapid flow, at maximum rates of ~70 nm/s, consistent with the unloaded speed of nonmuscle myosin II measured in vitro (Cuda *et al.*, 1997). This retrograde flow decayed fourfold as cellular force generation increased. During this time, thin bundles formed in the lamellar network and focal adhesions elongated. The changes in dynamics suggest that, during this stage, myosin motors rapidly contract an actin meshwork until they stall. An estimation of the stall force of myosin motors in the cell is approximated by $F_{cell} \sim F_s A n_{puncta} N_{myosin}$, where F_s is the stall force of the motor, A is the cell area, n_{puncta} is the density of myosin puncta in the lamella, and N_{myosin} is the number of myosin motors per puncta. Indeed using experimentally measured values of A ~ 3600 μm^2 and n_{puncta} ~ 1 puncta/μm^2 along with reported estimates of F_s ~ 2 pN (Molloy *et al.*, 1995) and N_{myosin} ~ 20 (Niederman and Pollard, 1975; Verkhovsky and Borisy, 1993), the number we obtain is on the order of 80–100 nN, consistent with the total cellular traction exerted at this time. We speculate that this stall force sets the transition when retrograde flow is stabilized and remodeling of the network into bundles commences. Thus over half of the total force output of the cell can be obtained through modifications to retrograde flow dynamics of a contractile lamellar actomyosin network (Figure 7).

When the retrograde flow of actin and myosin flow stabilizes, lamellar actin is remodeled into a network of stress fibers spanning the lamella and cell body (Figure 7). This remodeling requires sufficiently stiff ECM and is correlated to moderate changes in cellular tension over long time scales. During this period, both the number of actin bundles increases and individual bundles thicken. During bundle thickening, bundles accumulate actin, myosin band spacing decreases, and α-actinin bands form and intensify. At the highest levels of cellular tension, a network of stress fibers with alternating bands of α-actinin and myosin with a spacing of ~1 μm is formed.

Our data strongly suggest a model of stress fiber formation whereby myosin remodels actin into thin bundles, which then promotes the accumulation of α-actinin. We speculate that myosin-mediated alignment of F-actin into compact parallel and/or antiparallel filaments facilitates the enhanced binding of α-actinin, which favors the binding of closely spaced F-actin (Bartles, 2000). Future work is required to test this speculation and to rule out other mechanisms of α-actinin recruitment. Our model contrasts previous models, which suggest that α-actinin bundling of F-actin precedes the incorporation of myosin (Hotulainen and Lappalainen, 2006). One possibility for this difference is that previous experiments studied stress fiber formation near the leading cell edge. Near the leading edge, stress fiber assembly occurs rapidly within a small region. Thus low-tension actomyosin dynamics and organization could be difficult to assess.

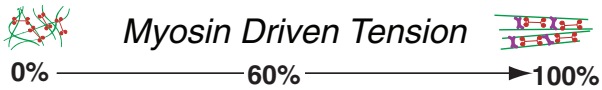

Actin Organization	Network	Stress Fibers form + thicken
Myosin bands	random	~2 μm → ~1 μm
α-actinin bands	N/A	form + intensify ~1.5 μm → ~1 μm
Dynamics	25 nm/s → 5 nm/s	5 nm/s

FIGURE 7: Correlation between cellular tension states and changes in cytoskeletal organization and dynamics. At low tension and rapid time scales, increased cellular force generation is inversely correlated to retrograde flow dynamics in a contractile actin network. At higher tension and slower time scales, retrograde flow stabilizes and F-actin bundles form and thicken. During bundle thickening, both actin and α-actinin bands intensify and the band spacing decreases from ~2 to ~1 μm. At the highest tension, stress fibers composed of α-actinin and myosin bands with a spacing of ~1 μm are formed.

We speculate that the mechanisms for remodeling of the lamellar meshwork into actin bundles is likely to occur both by the realignment of preexisting F-actin into bundles by myosin (Verkhovsky *et al.*, 1995) and by the polymerization dynamics of F-actin (Hotulainen and Lappalainen, 2006). Although it is difficult to directly assess the former, photobleaching measurements have shown that actin in lamellar contractile networks turns over quite rapidly (~30 s), making it unlikely that individual actin filaments are stable during the 10 min of bundle assembly and that mechanisms to promote actin assembly along the entire bundle length during thickening are necessary. Dissecting the molecular mechanisms that control this accretion process requires future work.

A surprising result stemming from our study is that a significant amount of force can be generated in a contractile lamellar network absent of stress fibers. Moreover, this force generation appears to be unaffected by changes in ECM compliance. This finding suggests that one must reconsider the assumptions of a cellular contractile state based solely on the prevalence of stress fibers. We speculate that the contractile lamellar networks may allow for rapid tuning of cytoskeletal tension in response to changes in external or internal forces over second time scales. By contrast, the slow dynamics of stress fiber assembly may not facilitate such rapid tuning.

Our results reveal a continuum of actomyosin organizations at different levels of tension with contractile lamellar networks and networks of stress fibers characterizing the lower and upper bounds, respectively. These bounds can be described by common cell types, such as keratocytes or Ptk1 cells, which exert low levels of force and tend to form contractile lamellar networks (Theriot and Mitchison, 1991; Lee *et al.*, 1994), and fibroblasts, which can exert high levels of force and typically display abundant stress fibers (Pelham and Wang, 1997; Balaban *et al.*, 2001; Tan *et al.*, 2003). Consistent with our data, traction forces in keratocytes and Ptk1 cells are largely regulated by actin dynamics (Gardel *et al.*, 2008; Fournier *et al.*, 2010), consistent with several recent models of actomyosin contractility (Kruse *et al.*, 2006; Rubinstein *et al.*, 2009). By contrast, we expect forces in stress fiber–rich cells to be regulated by structural effects, as speculated by other models of cellular force generation (Bischofs *et al.*, 2008). Our results indicate that both types of models are needed to capture the biophysical behavior over a large range of forces and, ideally, these would be integrated to take into account large rearrangements in forces observed during dynamic cellular processes. From this, a coherent biophysical understanding of force generation by the actomyosin cytoskeleton will likely emerge.

MATERIALS AND METHODS

Cell culture and transfection

Human osteosarcoma (U2OS) cells were obtained from the American Type Culture Collection and maintained in McCoy's medium (Hyclone Thermo Scientific, Rockford, IL), supplemented with 10% fetal bovine serum (HyClone), penicillin, and streptomycin (Life Technologies, Carlsbad, CA). Transient transfections of GFP-actin, GFP-α-actinin (C. Waterman, National Institutes of Health), mApple-actin, mApple-paxillin, and GFP-MLC (M. Davidson, University of Florida) were performed with FuGENE6 Transfection Reagent (Roche, Madison, WI) per manufacturer's instructions.

Preparation of polyacrylamide (PAA) substrates for traction force microscopy

Fibronectin-coated PAA substrates containing 40-nm fluorescent spheres were prepared on glass coverslips (Gardel *et al.*, 2008; Sabass *et al.*, 2008) with an acrylamide/*bis*-acrylamide ratio of 7.5/0.1% to obtain gels with a shear elastic moduli of 2.8 kPa and 5/0.075% for a shear elastic modulus of 0.6 kPa, as characterized previously (Aratyn-Schaus and Gardel, 2010). Fibronectin was covalently attached to the top surface of the PAA gel by utilizing the bifunctional cross-linker sulfo-SANPAH (Pierce Thermo Scientific, Rockford, IL).

Live-cell microscopy

Coverslips containing transfected cells bound to PAA substrates were mounted in a perfusion chamber (Warner Instruments, Hamden, CT) in imaging media consisting of culture media supplemented with 30 μl/1 ml Oxyrase (Oxyrase Enzyme system, EC0050) and 10 mM HEPES, pH 7.5. Cells were imaged at 37°C, 24–48 h posttransfection, on a multispectral spinning-disk confocal microscope consisting of a Nikon Ti with a 60× 1.2 NA plan Apo WI objective (Nikon, Melville, NY) through a CSUX spinning-disk head (Yokogawa, Sugar Land, TX) using a charge-coupled device camera (Coolsnap HQ2; Photometrics, Tucson, AZ). The microscope was controlled with Metamorph acquisition software (MDS Analytical Technologies, Sunnyvale, CA). Focal adhesions and beads were monitored at the same confocal section; F-actin, myosin light chain, and α-actinin were imaged 0.2 μm into the cell interior.

Cells were treated with 50 μM blebbistatin (Sigma, St. Louis, MO) for 30 min (Aratyn-Schaus and Gardel, 2010). To inactivate blebbistatin, cells were washed with imaging media and visualized with 488-nm light (Sakamoto *et al.*, 2005).

Image analysis

Particle Imaging Velocimetry code in MATLAB (mpiv, http://www.oceanwave.jp/softwares/mpiv/) was used to identify, with subpixel accuracy, the movement of beads embedded in PAA substrate. Fourier transform traction cytometry methods were used to determine the traction stress from bead displacements (Sabass *et al.*, 2008). The total cellular traction force was calculated by summing the force per unit area, obtained from the traction stress vector magnitude, across the entire cell. Fiducial marks of GFP-MLC were tracked using computational tracking software

developed at the laboratory of G. Danuser (Ji and Danuser, 2005). To evaluate the location of myosin puncta along bundles over time, kymographs were created using line scans across bundles that were aligned in the bundle reference frame.

Calculation of total cellular force

Force was calculated by multiplying the sum of stresses per unit area by the total cell area. The force recovery data indicate the normalized recovery profiles for data taken after blebbistatin removal, with data normalized to the total traction force recovered.

Measurement of band spacing

Band spacing was determined by averaging the center-to-center spacing between neighboring fluorescent bands, containing either GFP-tagged myosin or α-actinin, along stress fibers.

Linear density of actin bundles

Line scans of 10-μm length and 2-μm width were drawn perpendicular to F-actin bundles. Background-subtracted fluorescence profiles revealed series of peaks and troughs, with actin bundles identified by peaks with a full width at half maximum of approximately seven pixels. The value of I_b/I_c was calculated by taking the ratio of the background-subtracted peak intensity to the surrounding cytoplasm. This method was repeated for calculating the linear density of α-actinin bands within bundles, with the intensity profile given by GFP-α-actinin.

Curve fitting

Recovery profiles were fit using a least-squares minimization to either a first-order exponential function, $y = y_0 + A^{(-t/k)}$, or a second-order exponential function, $y = y_0 + A_1^{(-t/k_1)} + A_2^{(-t/k_2)}$, with offset value y_0; constants A, A_1, and A_2; and exponential constants, k, k_1, and k_2.

Order parameter calculation

Images were prefiltered using a series of elongated Laplace of Gaussian filters to create a maximum response image as described by Zemel *et al.* (2010). Local directions of alignment were then determined by breaking the image down into a grid of small overlapping windows. We used a window size of 31 × 31 pixels, with the centers of the windows spaced 5 pixels apart. The window was then convolved with a Gaussian filter and the two-dimensional fast Fourier transform (FFT) of the window was calculated. The Gaussian filter applied to the window before the FFT reduced the noise created by edge effects of the two-dimensional FFT. A series of line scans determined the direction of skew in the transform, which is perpendicular to the direction of alignment in real space. Correlations in alignment were determined by comparing the direction of alignment for a given window with its neighboring windows by examining the average of the second Legendre polynomial, a technique traditionally used to measure alignment in liquid crystals (de Gennes, 1974):

$$\left\langle \frac{1}{2}\left(3\cos^2\theta - 1\right)\right\rangle.$$

For the data presented here, the average was taken over a 7 × 7 box of neighboring grid points, with θ measured in reference from the direction defined at the center of the box. High values reveal regions where there is local correlation in alignment (i.e., more bundles all in the same direction). Low values indicate regions of random or noisy alignment. As the extent of actin bundles in the cell increases we see an increase in local measures of alignment.

ACKNOWLEDGMENTS

The authors acknowledge the use of computational analysis algorithms to analyze cytoskeletal dynamics and traction forces developed in the laboratories of Gaudenz Danuser and Ulrich Schwarz, respectively. The authors thank Yvonne Beckham for helpful comments and careful reading of the manuscript. This work was supported by a Burroughs Wellcome Career Award, Packard Fellowship, and NIH Director's Pioneer Award (DP10D00354) to M.L. Gardel, as well as the Keck Initiative for Ultrafast Imaging at the University of Chicago.

REFERENCES

Alexandrova AY, Arnold K, Schaub S, Vasiliev JM, Meister JJ, Bershadsky AD, Verkhovsky AB (2008). Comparative dynamics of retrograde actin flow and focal adhesions: formation of nascent adhesions triggers transition from fast to slow flow. PLoS ONE 3, e3234.

Aratyn-Schaus Y, Gardel ML (2010). Transient frictional slip between integrin and the ECM in focal adhesions under myosin II tension. Curr Biol 20, 1145–1153.

Balaban NQ *et al.* (2001). Force and focal adhesion assembly: a close relationship studied using elastic micropatterned substrates. Nat Cell Biol 3, 466–472.

Bartles JR (2000). Parallel actin bundles and their multiple actin-bundling proteins. Curr Opin Cell Biol 12, 72–78.

Beningo KA, Hamao K, Dembo M, Wang YL, Hosoya H (2006). Traction forces of fibroblasts are regulated by the Rho-dependent kinase but not by the myosin light chain kinase. Arch Biochem Biophys 456, 224–231.

Bershadsky AD, Balaban NQ, Geiger B (2003). Adhesion-dependent cell mechanosensitivity. Annu Rev Cell Dev Biol 19, 677–695.

Bischofs IB, Klein F, Lehnert D, Bastmeyer M, Schwarz US (2008). Filamentous network mechanics and active contractility determine cell and tissue shape. Biophys J 95, 3488–3496.

Burridge K, Chrzanowska-Wodnicka M (1996). Focal adhesions, contractility, and signaling. Annu Rev Cell Dev Biol 12, 463–518.

Choi CK, Vicente-Manzanares M, Zareno J, Whitmore LA, Mogilner A, Horwitz AR (2008). Actin and alpha-actinin orchestrate the assembly and maturation of nascent adhesions in a myosin II motor-independent manner. Nat Cell Biol 10, 1039–1050.

Chrzanowska-Wodnicka M, Burridge K (1996). Rho-stimulated contractility drives the formation of stress fibers and focal adhesions. J Cell Biol 133, 1403–2013.

Cramer LP (1999). Organization and polarity of actin filament networks in cells: implications for the mechanism of myosin-based cell motility. Biochem Soc Symp 65, 173–205.

Cuda G, Pate E, Cooke R, Sellers JR (1997). In vitro actin filament sliding velocities produced by mixtures of different types of myosin. Biophys J 72, 1767–1779.

de Gennes PG (1974). The Physics of Liquid Crystals, Oxford, UK: Clarendon Press.

Discher DE, Janmey P, Wang Y-l (2005). Tissue cells feel and respond to the stiffness of their substrate. Science 310, 1139–1143.

Fournier MF, Sauser R, Ambrosi D, Meister JJ, Verkhovsky AB (2010). Force transmission in migrating cells. J Cell Biol 188, 287–297.

Gardel ML, Sabass B, Ji L, Danuser G, Schwarz US, Waterman CM (2008). Traction stress in focal adhesions correlates biphasically with actin retrograde flow speed. J Cell Biol 183, 999–1005.

Gardel ML, Schneider IC, Aratyn-Schaus Y, Waterman CM (2010). Mechanical integration of actin and adhesion dynamics in cell migration. Annu Rev Cell Dev Biol 26, 3.1–3.19.

Geiger B, Spatz JP, Bershadsky AD (2009). Environmental sensing through focal adhesions. Nat Rev Mol Cell Biol 10, 21–33.

Giannone G, Dubin-Thaler BJ, Dobereiner HG, Kieffer N, Bresnick AR, Sheetz MP (2004). Periodic lamellipodial contractions correlate with rearward actin waves. Cell 116, 431–443.

Hotulainen P, Lappalainen P (2006). Stress fibers are generated by two distinct actin assembly mechanisms in motile cells. J Cell Biol 173, 383–394.

Hu K, Ji L, Applegate KT, Danuser G, Waterman-Storer CM (2007). Differential transmission of actin motion within focal adhesions. Science 315, 111–115.

Ji L, Danuser G (2005). Tracking quasi-stationary flow of weak fluorescent signals by adaptive multi-frame correlation. J Microsc 220, 150–167.

Katoh K, Kano Y, Ookawara S (2007). Rho-kinase dependent organization of stress fibers and focal adhesions in cultured fibroblasts. Genes Cells 12, 623–638.

Kruse K, Joanny JF, Julicher F, Prost J (2006). Contractility and retrograde flow in lamellipodium motion. Phys Biol 3, 130–137.
Lee J, Leonard M, Oliver T, Ishihara A, Jacobson K (1994). Traction forces generated by locomoting keratocytes. J Cell Biol 127, 1957–1964.
Molloy JE, Burns JE, Kendrick-Jones J, Tregear RT, White DC (1995). Movement and force produced by a single myosin head. Nature 378, 209–212.
Naumanen P, Lappalainen P, Hotulainen P (2008). Mechanisms of actin stress fibre assembly. J Microsc 231, 446–454.
Niederman R, Pollard TD (1975). Human platelet myosin. II. In vitro assembly and structure of myosin filaments. J Cell Biol 67, 72–92.
Parsons JT, Horwitz AR, Schwartz MA (2010). Cell adhesion: integrating cytoskeletal dynamics and cellular tension. Nat Rev Mol Cell Biol 11, 633–643.
Pelham RJ Jr, Wang Y (1997). Cell locomotion and focal adhesions are regulated by substrate flexibility. Proc Natl Acad Sci USA 94, 13661–13665.
Peterson LJ, Rajfur Z, Maddox AS, Freel CD, Chen Y, Edlund M, Otey C, Burridge K (2004). Simultaneous stretching and contraction of stress fibers in vivo. Mol Biol Cell 15, 3497–3508.
Rubinstein B, Fournier MF, Jacobson K, Verkhovsky AB, Mogilner A (2009). Actin-myosin viscoelastic flow in the keratocyte lamellipod. Biophys J 97, 1853–1863.
Sabass B, Gardel ML, Waterman CM, Schwarz US (2008). High resolution traction force microscopy based on experimental and computational advances. Biophys J 94, 207–220.
Sakamoto T, Limouze J, Combs CA, Straight AF, Sellers JR (2005). Blebbistatin, a myosin II inhibitor, is photoinactivated by blue light. Biochem 44, 584–588.
Schaub S, Bohnet S, Laurent VM, Meister J-J, Verkhovsky AB (2007). Comparative maps of motion and assembly of filamentous actin and myosin II in migrating cells. Mol Biol Cell 18, 3723–3732.
Straight AF, Cheung A, Limouze J, Chen I, Westwood NJ, Sellers JR, Mitchison TJ (2003). Dissecting temporal and spatial control of cytokinesis with a myosin II inhibitor. Science 299, 1743–1747.
Svitkina TM, Verkhovsky AB, McQuade KM, Borisy GG (1997). Analysis of the actin-myosin II system in fish epidermal keratocytes: mechanism of cell body translocation. J Cell Biol 139, 397–415.
Tan JL, Tien J, Pirone DM, Gray DS, Bhadriraju K, Chen CS (2003). Cells lying on a bed of microneedles: an approach to isolate mechanical force. Proc Natl Acad Sci USA 100, 1484–1489.
Theriot JA, Mitchison TJ (1991). Actin microfilament dynamics in locomoting cells. Nature 352, 126–131.
Vallotton P, Gupton SL, Waterman-Storer CM, Danuser G (2004). Simultaneous mapping of filamentous actin flow and turnover in migrating cells by quantitative fluorescent speckle microscopy. Proc Natl Acad Sci USA 101, 9660–9665.
Verkhovsky AB, Borisy GG (1993). Non-sarcomeric mode of myosin II organization in the fibroblast lamellum. J Cell Biol 123, 637–652.
Verkhovsky AB, Svitkina TM, Borisy GG (1995). Myosin II filament assemblies in the active lamella of fibroblasts: their morphogenesis and role in the formation of actin filament bundles. J Cell Biol 131, 989–1002.
Verkhovsky AB, Svitkina TM, Borisy GG (1997). Polarity sorting of actin filaments in cytochalasin-treated fibroblasts. J Cell Sci 110 (pt 15), 1693–1704.
Yeung T, Georges PC, Flanagan LA, Marg B, Ortiz M, Funaki M, Zahir N, Ming W, Weaver V, Janmey PA (2005). Effects of substrate stiffness on cell morphology, cytoskeletal structure, and adhesion. Cell Motil Cytoskeleton 60, 24–34.
Zemel A, Rehfeldt F, Brown AE, Discher DE, Safran SA (2010). Optimal matrix rigidity for stress fiber polarization in stem cells. Nat Phys 6, 468–473.
Zhang X, Jiang G, Cai Y, Monkley SJ, Critchley DR, Sheetz MP (2008). Talin depletion reveals independence of initial cell spreading from integrin activation and traction. Nat Cell Biol 10, 1062–1068.